Free Vibration Analysis of 2D Functionally Graded Annular Plate considering the Effect of Material Composition via 2D Differential Quadrature Method

M. Nejati[a], H. Mohsenimonfared[b]*, A. Asanjarani[a]

[a]*Young Researchers and Elite Club, Islamic Azad University, Arak Branch, Arak, Iran*

[b]*Department of Mechanical Engineering, Islamic Azad University, Arak Branch, Arak, Iran*

ABSTRACT

This study investigates the free vibration of the Two-Dimensional Functionally Graded Annular Plates (2D-FGAP). The theoretical formulations are based on the three-dimensional elasticity theory with small strain assumption. The Two-Dimensional Generalized Differential Quadrature Method (2D-GDQM) as an efficient and accurate semi-analytical approach is used to discretize the equations of motion and to implement the various boundary conditions. The fast rate of convergence for this method is shown and the results are compared with the existing results in the literature. The material properties are assumed to be continuously changing along thickness and radial directions simultaneously, which can be varied according to the power law and exponential distributions, respectively. The effects of the geometrical parameters, the material graded indices in thickness and radial directions, and the mechanical boundary conditions on the frequency parameters of the two-dimensional functionally graded annular plates are evaluated in detail. The results are verified to be against those given in the literature.

1. Introduction

In the last decade, the Functionally Graded Materials (FGMs) were employed in various engineering applica-tions and were first reported in 1984 by Japanese material scientists [1]. The FGMs are het-erogeneous materials in which, the thermo-mechanical properties vary con-tinuously and generally as a function of position throughout the material. A typical FGM is created by smoothly changing the volume fraction of its materials constituents.

This new type of materials can be applied to avoid in-terfacial stress concentration appeared in laminated struc-tures, and therefore, a great promise is proposed by FGMs in applications where the working conditions are severe[2], including spacecraft heat shields, heat ex-changer tubes, plasma facings for fusion reactors, engine components and high-power electrical contacts or even magnets.

Compared with the analysis of functionally graded rectangular plates [3-11] and functionally graded spheres [12] as well as functionally graded cylindrical shells [13-17], the investigations of functionally graded annular plates are limited in number. Moreover, the proposed semi-analytical 2D-GDQ has led to obtain more accurate results with appropriate rate of convergence. Prakash and Ganapathi [18] investigated the asym-metric free vibration behaviours and the thermo-elastic stability of the functionally graded circular plates based on the first-order shear deformation theory using the finite element method. The material properties were supposed graded in the thickness direction according to the simple power law distribution. Eraslan and Akis

---

*Corresponding author, Tel.: +98-918-1623597; fax: +98-863-4173450

E-mail address: h-mohsenimonfared@iau-arak.ac.ir

[19] obtained the closed form solution of the functionally graded rotating solid shaft and rotating solid disks under the generalized plane strain and plane stress assumptions, respectively. Efraim and Eisenberger [20] investigated the FGM plate with the material properties varying smoothly through the thickness of the plate. The equations of motion including the effect of shear deformations using the First-order Shear Deformation Theory (FSDT) were derived and solved exactly for various arrangements of the boundary conditions. The solution was obtained.

Nie and Zhong [21] studied the three – dimensional vibration of the functionally graded circular plates using the semi-analytical approach. The dynamic analysis of the multi-directional functionally graded annular plates was obtained using the state space-based differential quadrature method based on the three-dimensional elastic theory and on the assumption that the material properties have an exponent-law variation along the thickness, radial direction or both directions. Dong [22] studied the three-dimensional free vibration of functionally graded annular plates with various boundary conditions using the Chebyshev–Ritz method. Two types of variations were considered for the material properties in the thickness direction of the plates. Yas and Tahouneh [23] studied the free vibration of the functionally graded annular plates based on the elastic foundations, using the differential quadrature method for various boundary conditions. The foundation was defined by Pasternak or a two-parameter model. A semi-analytical method composed of Differential Quadrature Method (DQM) and series solution are em-ployed to solve the equations of motions. The material properties were continuously varied through the thickness of the plate. Hosseini-Hashemi et al. [24] presented a solution to investigate the free vibration analysis of the radially functionally graded circular and annular sector thin plates of variable thickness based on the Classical Plate Theory (CPT) using the Differential Quadrature Method (DQM).

Jodaei et al. [25] presented a three-dimensional anal-ysis of functionally graded annular plates using State-Space based Differential Quadrature Method (SSDQM) and a comparative behaviour modelling using Artificial Neural Network (ANN) for various boundary conditions. The material properties were supposed to have an exponent-law variation along the thickness. Malekzadeh et al. [26] studied the free vibration of Functionally Graded (FG) thick annular plates subjected to thermal environment based on the 3D elasticity theory. The material properties were assumed to be temperature dependent and graded in the thickness direction. The Differential Quadrature Method (DQM) as an efficient and accurate numerical tool was used to solve both the thermo-elastic equilibrium and the free vibration equations.

Behravan Rad and Shariyat [27] investigated the bending and stress analyses of the two-directional Functionally Graded (FG) annular plates resting on the non-uniform two-parameter Winkler-Pasternak foundations, subjected to the normal and in-plane-shear tractions using the exact three-dimensional theory of elasticity. The solution was obtained by employing the state space and differential quadrature methods. The material properties were assumed to vary in both transverse and radial directions. Three different types of variations of the stiffness of the foundation were considered in the radial direction: linear, parabolic, and sinusoidal. Malekzadeh and Safaeian [28] employed a three-dimensional (3D) discrete layer approach coupled with the Differential Quadrature Method (DQM) to investigate the free vibration analysis of the laminated Functionally Graded (FG) annular plates subjected to a thermal environment. The formulations were derived from the elasticity theory, which included the effects of the initial thermal stresses. Liang et al. [29] studied the transient response of the FGM annular sector plate with arbitrary circular boundary conditions based on the semi-analytical methodology. The FGM annular sector plate was simply supported at the radial edges. At the circular edges, four kinds of boundary conditions were considered: Clamped–Clamped, Clamped–Simply supported, Clamped–Free and Simply supported–Simply supported. The results obtained in this study can be served as the benchmark data for further researches.

To the best of the author's knowledge, the 2D generalized quadrature method has not been yet employed to study the free vibration of the 2D functionally graded annular plates. Therefore, the purpose of this study is to investigate the free vibration analysis of the considered 2D-FG annular plate. It is supposed that the plate rests on different boundary conditions namely simply-simply, clamped-clamped, simply-clamped as well as free-clamped on the inner and outer edges, re-spectively. The equations of the motion are obtained according to a 3D-elasticity theory which ultimately. They are reduced to the coupled differential equations. Con-sequently, a semi-analytical formulation based on a two-dimensional GDQ approach for the considered system of differential equations is derived, which results in determination of the frequency parameters. The material properties are assumed to be continuously changing along the thickness and radial directions simultaneously and affect the material composition, which can be varied according to the power law and exponential distributions, which in turn are

evaluated in details and compared with each other. Also, the rate of convergence for the 2D-GDQ is compared with other numerical methods.

2. Basic Equations

2.1 Governing equations

The equations of motion in the cylindrical coordinate system have to be formulated, in order to employ the so-called numerical procedure 2D-GDQ. For this purpose, it is supposed that the 2D-FG annular plate has the inner radial r_i, outer radial r_o and thickness h, with respect to the cylindrical coordinates (r, θ, z) attached on the bottom of the plate (Fig. 1). In the form of the cylindrical coordinate system, the linear strain-displacement relations are employed as follows:

$$\varepsilon_r = \frac{\partial U_r}{\partial r}, \varepsilon_\theta = \frac{U_r}{r} + \frac{1}{r}\frac{\partial U_\theta}{\partial \theta}, \varepsilon_z = \frac{\partial U_z}{\partial z}$$

$$\gamma_{r\theta} = \frac{1}{r}\frac{\partial U_r}{\partial \theta} + \frac{\partial U_\theta}{\partial r} - \frac{U_\theta}{r}, \gamma_{rz} = \frac{\partial U_r}{\partial z} + \frac{\partial U_z}{\partial r},$$

$$\gamma_{z\theta} = \frac{\partial U_\theta}{\partial z} + \frac{1}{r}\frac{\partial U_z}{\partial \theta}$$

(1)

where U_r, U_θ and U_z are displacement components toward radial, circumferential and thickness directions and $\varepsilon_r, \varepsilon_\theta, \varepsilon_z$ are the corresponding axial strain components and $\gamma_{r\theta}, \gamma_{rz}, \gamma_{z\theta}$ are in-plane and out-of-plane shear strain components, respectively. In the absence of the body forces, the equations of motion are obtained according to Eq. (2):

$$\frac{\partial \sigma_r}{\partial r} + \frac{1}{r}\frac{\partial \sigma_{r\theta}}{\partial \theta} + \frac{\partial \sigma_{rz}}{\partial z} + \frac{\sigma_r - \sigma_\theta}{r} = \rho\frac{\partial^2 u_r}{\partial t^2}$$

$$\frac{\partial \sigma_{r\theta}}{\partial r} + \frac{1}{r}\frac{\partial \sigma_\theta}{\partial \theta} + \frac{\partial \sigma_{z\theta}}{\partial z} + \frac{2\sigma_{r\theta}}{r} = \rho\frac{\partial^2 u_\theta}{\partial t^2}$$

(2)

$$\frac{\partial \sigma_{rz}}{\partial r} + \frac{1}{r}\frac{\partial \sigma_{z\theta}}{\partial \theta} + \frac{\partial \sigma_z}{\partial z} + \frac{\sigma_{rz}}{r} = \rho\frac{\partial^2 u_z}{\partial t^2}$$

where σ_r, σ_θ and σ_z are axial stress components, and $\sigma_{r\theta}, \sigma_{rz}$ and $\sigma_{z\theta}$ are shear stress components. Apparently, ρ denotes material density and t refers to time, here.
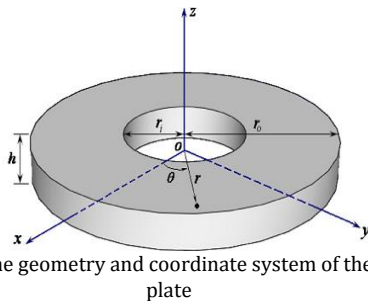
Figure 1. The geometry and coordinate system of the annular plate

The stress-strain relations for the mentioned isotropic FGM are obtained according to the generalized Hook's law as follows:

$$\begin{Bmatrix} \sigma_r \\ \sigma_\theta \\ \sigma_z \\ \sigma_{z\theta} \\ \sigma_{rz} \\ \sigma_{r\theta} \end{Bmatrix} = \begin{bmatrix} C_{11} & C_{12} & C_{13} & 0 & 0 & 0 \\ C_{12} & C_{22} & C_{23} & 0 & 0 & 0 \\ C_{13} & C_{23} & C_{33} & 0 & 0 & 0 \\ 0 & 0 & 0 & C_{44} & 0 & 0 \\ 0 & 0 & 0 & 0 & C_{55} & 0 \\ 0 & 0 & 0 & 0 & 0 & C_{66} \end{bmatrix}\begin{Bmatrix} \varepsilon_r \\ \varepsilon_\theta \\ \varepsilon_z \\ \gamma_{z\theta} \\ \gamma_{rz} \\ \gamma_{r\theta} \end{Bmatrix}$$

(3)

where C_{ij} denotes compliance for the isotropic FGM. The displacement fields U_r, U_θ and U_z for the free vibration of 2D-FG annular plates are represented as unknown functions along the radial and thickness directions and known trigonometric functions along the circumferential direction as follows:

$$U_r(r,\theta,z,t) = u_{rm}(r,z)\cos(m\theta)e^{i\omega_m t}$$

$$U_\theta(r,\theta,z,t) = u_{\theta m}(r,z)\sin(m\theta)e^{i\omega_m t}$$

(4)

$$U_z(r,\theta,z,t) = u_{zm}(r,z)\cos(m\theta)e^{i\omega_m t}$$

where m denotes the circumferential wave-number which could specify any positive integer values $(m=0,1,...,\infty)$. ω is the natural frequency parameter and i is the imaginary number. It is obvious that $m = 0$ means axisymmetric vibration. Combining the strain-displacement relations Eq. (1) into the Hook's law Eq. (3) and substituting into the equations of motion Eq. (2) and then using the trigonometric functions Eq. (4) leads to what follows:

$$\frac{\partial C_{11}}{\partial r}\frac{\partial u_{rm}}{\partial r} + C_{11}\frac{\partial^2 u_{rm}}{\partial r^2} + \frac{\partial C_{12}}{\partial r}\left(\frac{u_{rm}}{r} + \frac{1}{r}u_{\theta m}m\right) + \frac{\partial C_{13}}{\partial r}\frac{\partial u_{zm}}{\partial z}$$

$$+ C_{13}\frac{\partial^2 u_{zm}}{\partial r\partial z} + \frac{C_{11}-C_{12}}{r}\frac{\partial u_{rm}}{\partial r} + C_{12}\left(\frac{1}{r}\frac{\partial u_{rm}}{\partial r} + \frac{1}{r}\frac{\partial u_{\theta m}}{\partial r}m\right) -$$

$$C_{12}\left(\frac{u_{rm}}{r^2} + \frac{1}{r^2}u_{\theta m}m\right) + \frac{C_{66}}{r}\left(-\frac{u_{\theta m}}{r}m + \frac{\partial u_{\theta m}}{\partial r}m - \frac{1}{r}u_{rm}m^2\right) +$$

$$\frac{\partial C_{55}}{\partial z}\left(\frac{\partial u_{rm}}{\partial z} + \frac{\partial u_{zm}}{\partial r}\right) + C_{55}\left(\frac{\partial^2 u_{rm}}{\partial z^2} + \frac{\partial^2 u_{zm}}{\partial r\partial z}\right) +$$

$$\frac{C_{12}-C_{22}}{r}\left(\frac{u_{rm}}{r} + \frac{1}{r}u_{\theta m}m\right) + \frac{C_{13}-C_{23}}{r}\frac{\partial u_{zm}}{\partial z} = -\rho\omega^2 u_{rm}$$

(5)

$$\frac{\partial C_{66}}{\partial r}\left(-\frac{u_{\theta m}}{r} + \frac{\partial u_{\theta m}}{\partial r} - \frac{1}{r}u_{rm}m\right) +$$

$$C_{66}\left(-\frac{1}{r}\frac{\partial u_{rm}}{\partial r}m - \frac{1}{r}\frac{\partial u_{\theta m}}{\partial r} + \frac{u_{\theta m}}{r^2} + \frac{\partial^2 u_{\theta m}}{\partial r^2} + \frac{1}{r^2}u_{rm}m\right) -$$

$$\frac{C_{12}}{r}\frac{\partial u_{rm}}{\partial r}m - \frac{C_{23}}{r}\frac{\partial u_{zm}}{\partial z}m - \frac{C_{22}}{r^2}\left(u_{rm}m + u_{\theta m}m^2\right) +$$

$$\frac{\partial C_{44}}{\partial z}\left(\frac{\partial u_{\theta m}}{\partial z} - \frac{1}{r}u_{zm}m\right) + C_{44}\left(\frac{\partial^2 u_{\theta m}}{\partial z^2} - \frac{1}{r}\frac{\partial u_{zm}}{\partial z}m\right) -$$

$$\frac{2C_{66}}{r^2}u_{rm}m + \frac{2C_{66}}{r}\frac{\partial u_{\theta m}}{\partial r} - \frac{2C_{66}}{r^2}u_{\theta m} = -\rho\omega^2 u_{\theta m}$$

(6)

$$\frac{\partial C_{55}}{\partial r}\left(\frac{\partial u_{rm}}{\partial z}+\frac{\partial u_{zm}}{\partial r}\right)+C_{55}\left(\frac{\partial^2 u_{zm}}{\partial r^2}+\frac{\partial^2 u_{rm}}{\partial r\partial z}\right)+$$

$$\frac{C_{44}}{r}\frac{\partial u_{\theta m}}{\partial z}m-\frac{C_{44}}{r^2}u_{zm}m^2+\frac{\partial C_{13}}{\partial z}\frac{\partial u_{rm}}{\partial r}+$$

$$C_{13}\frac{\partial^2 u_{rm}}{\partial r\partial z}+\frac{\partial C_{23}}{\partial z}\left(\frac{u_{rm}}{r}+\frac{1}{r}u_{\theta m}m\right)+$$

$$C_{23}\left(\frac{1}{r}\frac{\partial u_{rm}}{\partial z}+\frac{1}{r}\frac{\partial u_{\theta m}}{\partial z}m\right)+\frac{\partial C_{33}}{\partial z}\frac{\partial u_{zm}}{\partial z}+$$

$$C_{33}\frac{\partial^2 u_{zm}}{\partial z^2}+\frac{C_{55}}{r}\frac{\partial u_{rm}}{\partial z}+\frac{C_{55}}{r}\frac{\partial u_{zm}}{\partial r}=-\rho\omega^2 u_{zm}$$

$$(7)$$

Eqs. (5)-(7) denote 3D elasticity solution for the equations of motion in terms of the displacement components and must be solved for known compliances and assumptive displacement fields which have been supposed in Eq. (4). Then, it must be solved by employing the existing numerical procedure. Here, 2D-GDQ procedure has been considered to discretize the linear system of the equations Eqs. (5)-(7).

The Privileges of the 2D-GDQ approach compared with one-dimensional procedure are the types of boundary conditions and the grids distribution toward two directions which are illustrated in the following sections. In order to investigate the free vibration of 2D-FG annular plate resting on different foundations, four different kinds of boundary conditions are considered namely Clamped–Clamped (C-C), Simply supported –Clamped (S-C), Free-Clamped (F-C) and Simply supported–Simply supported(S-S). The boundary conditions at edges for the above mentioned foundations are as follows:
Clamped-Clamped (C-C):

$$r=r_i, r_o \quad u_r=u_\theta=u_z=0 \tag{8}$$

Simply supported – Clamped (S-C):

$$r=r_i \quad u_\theta=u_z=\sigma_r=0$$
$$r=r_o \quad u_r=u_\theta=u_z=0 \tag{9}$$

Free-Clamped (F-C):

$$r=r_i \quad \sigma_r=\sigma_{r\theta}=\sigma_{rz}=0$$
$$r=r_o \quad u_r=u_\theta=u_z=0 \tag{10}$$

Simply supported – Simply supported (S-S):

$$r=r_i, r_o \quad u_\theta=u_z=\sigma_r=0 \tag{11}$$

2.2 Micromechanics of the 2D-FGM annular plate

A typical FGM is made of two randomly distributed isotropic constituents, i.e. a metal and a ceramic. The macroscopic response of the FGM is isotropic and the compositions of the considered FGM vary throughout the radial and thickness directions.

Such a material allows continuous variation of the material composition. One important step in determining the micromechanical model of FG circular plate is homogenization. The approach should be chosen based on the gradient of composition relative to the size of a typical Representative Volume Element (RVE). Here, two kinds of materials distributions are employed. The first type is based on the exponential law distribution, and the second one is according to the power law distribution. The material elastic coefficients (C_{ij}) and the mass density (ρ) are assumed to have the following exponential law distribution along the thickness and radial directions of the plate as the following [30]:

$$C_{ij}(r,z)=C_{ij}(0,0)\exp(\lambda_1\frac{z}{h}+\lambda_2\frac{r}{r_o})$$
$$\rho(r,z)=\rho(0,0)\exp(\lambda_1\frac{z}{h}+\lambda_2\frac{r}{r_o}) \tag{12}$$

where $C_{ij}(0,0)$ and $\rho_{ij}(0,0)$ are the reference values at the center point of the bottom plane, and λ_1 and λ_2 denote the material property graded indexes in the thickness and radial directions, respectively.

In the first step, the material properties of the annular plate are assumed according to the exponent-law variation in the thickness and radial directions. Young's modulus at the center of the bottom plane is $E=380$ (GPa) and Poisson's ratio is chosen as constant ($v=0.3$). The material density at the center of the bottom plane equals $\rho=3800(Kg/m^3)$.

Defining the non-dimensional parameter $\varsigma=(z/h)-1/2$ in the thickness direction and $\eta=(r-R)/H$ in the radial directions, the density variation for different values of material property graded indexes is demonstrated in Fig. 2.

Where R is the average radius of annular plate and $H=r_o-r_i$. In case of power law distribution, we have annular plate which its inner and outer surfaces are made of two distinct ceramics and two distinct metals, respectively. C_1, C_2, M_1 and M_2 denote first ceramic, second ceramic, first metal and second metal, respectively. The volume fraction of the first ceramic material is varied from 100% at the lower surface to zero at the upper surface by a power law function. Also, this volume fraction is continuously varied from inner surface to the outer surface.
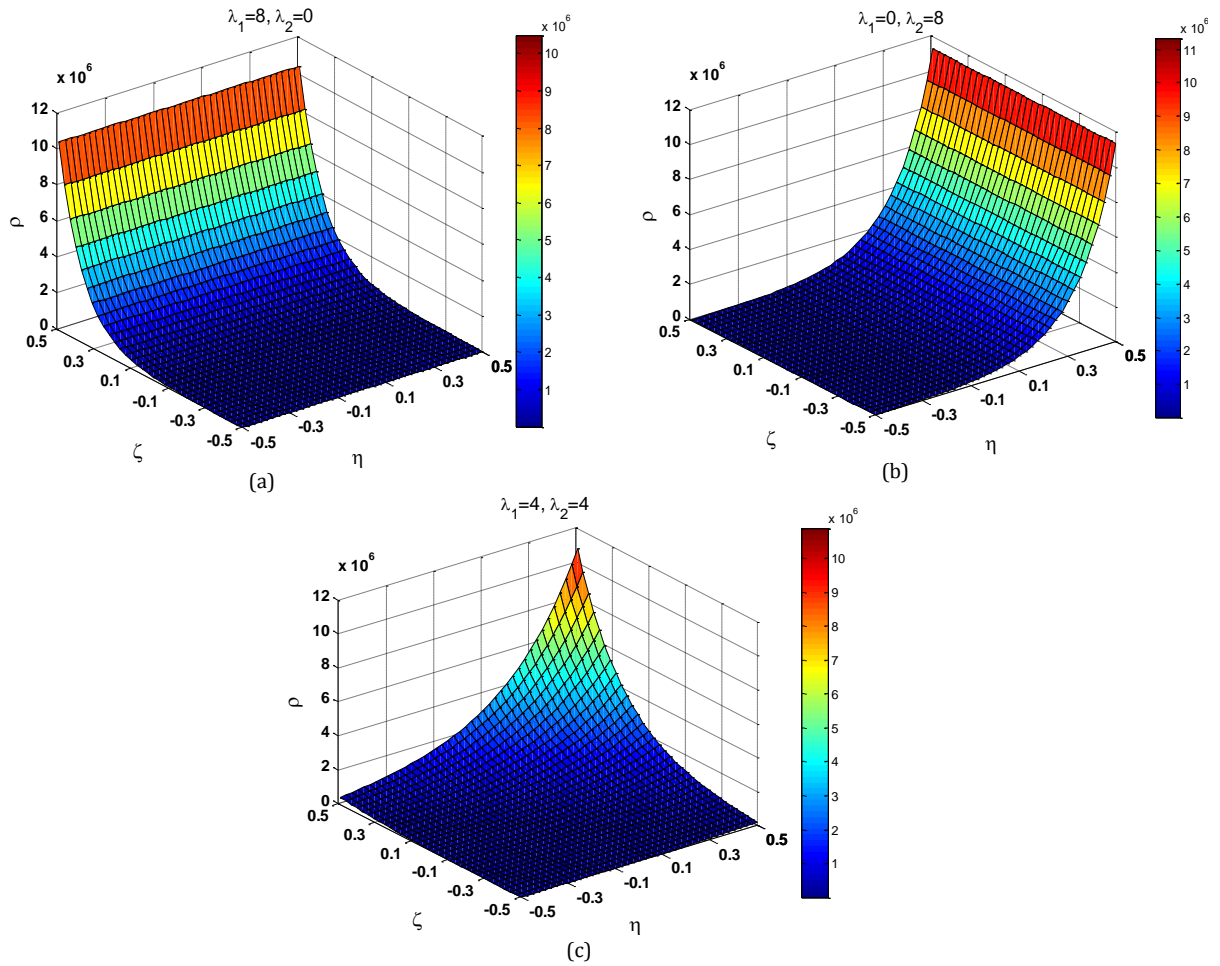
Figure 2. The density variation for (a) $\lambda_1 = 8$, $\lambda_2 = 0$ (b) $\lambda_1 = 0$, $\lambda_2 = 8$ and (c) $\lambda_1 = 4$, $\lambda_2 = 4$

The volume fractions of the other materials are changed in a similar way to the mentioned one in two directions. The volume fraction function of each material can be described as follows [31]:

$$V_{c1} = \left[1 - (\frac{r - r_i}{r_o - r_i})^{n_r}\right]\left[1 - (\frac{z}{h})^{n_z}\right]$$

$$V_{c2} = \left[1 - (\frac{r - r_i}{r_o - r_i})^{n_r}\right]\left[(\frac{z}{h})^{n_z}\right]$$

$$V_{m1} = (\frac{r - r_i}{r_o - r_i})^{n_r}\left[1 - (\frac{z}{h})^{n_z}\right] \tag{13}$$

$$V_{m2} = (\frac{r - r_i}{r_o - r_i})^{n_r}\left[(\frac{z}{h})^{n_z}\right]$$

where n_r, n_z are parameters representing the basic constituent distribution in r and z directions.

The effective material properties including elasticity modulus and density at each point can be obtained using the simple linear rule of mixtures, in which the mentioned material properties, E and ρ, at any arbitrary point (r, z) in the 2D-FGM annular plate are determined by a linear mixture of the volume fractions. The material properties of the basic

materials can be described as Eq. (14). It must be noted that, the Poisson's ratio is assumed to have a constant value.

$$E = E_{c1}V_{c1} + E_{c2}V_{c2} + E_{m1}V_{m1} + E_{m2}V_{m2}$$
$$\rho = \rho_{c1}V_{c1} + \rho_{c2}V_{c2} + \rho_{m1}V_{m1} + \rho_{m2}V_{m2} \tag{14}$$

where m and c subscripts stand for the metal and ceramic, respectively. The five different models section is configured in Fig. 3.

In this step, the effects of the FGM configuration are studied by investigating the natural frequencies of the five different FGM models as follows:

- Model (1): The 2D-FGM annular plate has ceramics on its inner surface and metals on its outer surface
- Model (2): The 2D-FGM annular plate has metal on its inner surface and ceramics on its outer surface
- Model (3): The 2D-FGM annular plate has ceramics on its bottom surface and metals on its upper surface
- Model (4): The 2D-FGM annular plate has metal on its bottom surface and ceramics on its upper surface
- Model (5): The 2D-FGM annular plate has ceramics on the corner at the left on the bottom surface, in the corner at the right on the upper surface and

metals on the corner at the right on the bottom surface, on the corner at the left on the upper surface.

The basic constituents of the 2D-FG annular plate for two kinds of distributions (exponential and power law) are presented in Table. 1 and it should be noted that the Poisson's ratio is assumed to be constant ($v = 0.3$).

Fig. 4 illustrates the distribution of the effective density of the 2D-FG plate versus two non-dimensional parameters ς and η for different values of the power exponents n_z and n_r.
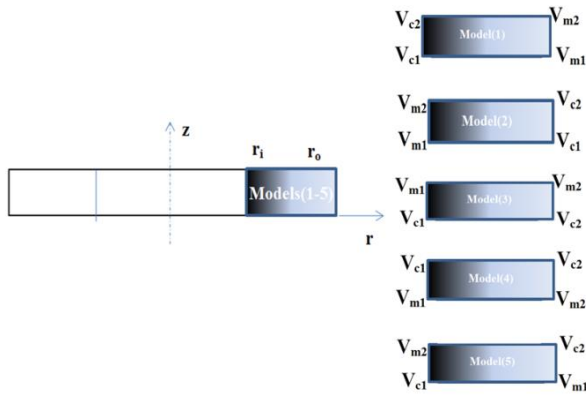
Figure 3. The FGM annular plate with the two-dimensional material distribution (Models 1-5)

Table 1. The material properties of the FGM plate for different distributions

Distribution	Constituents	E(GPa)	ρ (kg/m³)
Power-law distribution [31]	M_1	115	2715
	M_2	69	4515
	C_1	440	3210
	C_2	150	3470
Exponent-law distribution [30]	center point of the bottom plane	380	3800
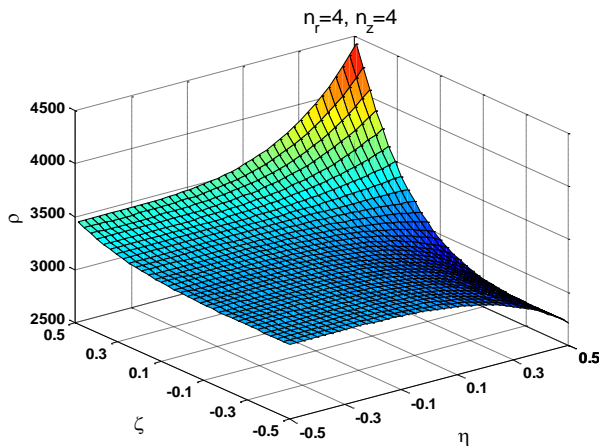
Figure 4. The distribution of the effective density for
$n_r = 4$, $n_z = 4$

2. Solution Procedure

It is difficult to solve the equations of motion analytically. Hence, one should use a numerical procedure in order to discretise the partial differential equations in terms of displacement components. Then, the set of discretized algebraic equation must be solved as an Eigen-value problem to find the natural frequencies. Apparently, Eqs. (5)-(7) are a linear set of the partial differential equations of motion which ought to be solved with one of the numerical solver. Here, the 2D-GDQ procedure is used to discretize the motion equations and followed by related boundary conditions. Choosing the solution procedure i.e. the 2D-GDQ method is first based on the type of boundary conditions and secon meshing the plate in two directions (Here the grids are distributed toward the material variations namely, the radial and thickness directions). The differential quadrature method (DQM) is a semi-analytical solution technique for initial and/or boundary value problems [32]. It was first developed by Richard Bellman and his associates in the early 1970s [33]. The DQ method is originated from the idea of conventional integral quadrature and approximates the derivative of a function at any discrete points by a weighted linear summation of the functional values in the whole domain [34]. A simple and accepted choice of the grid distribution is the uniform grid spacing rule; however, it is found that the non-uniform grid spacing yields results with a better accuracy. Hence, in this study, the Chebyshev–Gauss–Lobatto quadrature points are employed, the following equations are derived [32]:

$$\xi_i = \frac{1}{2}\left\{1 - \cos\left(\frac{\pi(i-1)}{N_r - 1}\right)\right\}, for \ i = 1,2,.., N_r \ and \ j = 1,2,..., N_z$$

$$\zeta_i = \frac{1}{2}\left\{1 - \cos\left(\frac{\pi(j-1)}{N_z - 1}\right)\right\}, for \ i = 1,2,.., N_r \ and \ j = 1,2,..., N_z$$

(15)

where ξ_i and ζ_i are the distribution of nodes along the *r* and *z* directions, respectively. As one can observe, with this non-homogeneous distribution of nodes, by approaching to the internal and external boundaries of the FGM annular plate with various boundary conditions and also the upper and lower boundaries with free boundary condition, the density of nodes increases while it causes the boundary conditions to be better satisfied. Getting far from boundaries, less density in the node of grid is generated. In the 2D-GDQ method, in order to approximate the first-order derivatives of the function $f(r,z)$ with respect to *r* in a node of grid, according to Eq. (16), the summation of multiplication of function values in all nodes in the *r* direction is parallel to the target node with the weighting coefficients in the direction *r*.

$$\frac{\partial f(r,z)}{\partial r} = \sum_{l=1}^{N_r} A_{jl}^{(r)} f_{lk} \qquad (16)$$

In order to obtain the weighting coefficients, a set of test functions should be employed. For the polynomial basis functions DQ, a set of Lagrange polynomials are employed as the test functions. The weighting coefficients for the first-order derivatives in *r*-direction can be described as follows [32]:

$$A_{jl}^{(r)} = \begin{cases} \dfrac{1}{L_r} \dfrac{M(\xi_j)}{(\xi_j - \xi_l)M(\xi_l)} & for \ j \neq l \\ -\displaystyle\sum_{\substack{l=1 \\ j \neq l}}^{N_r} A_{jl}^{(r)} & for \ j=l; \ j,l=1,2,....,N_r \end{cases} \qquad (17)$$

where L_r is the length of domain along the *r*-direction and

$$M(\xi_j) = \prod_{l=1, \ j\neq l}^{N_r} (\xi_j - \xi_l) \qquad (18)$$

According to the DQ method, for higher-order derivatives, higher-order weighting coefficient should be employed, i.e. for second-order derivatives, the weighting coefficient can be expressed as below:

$$B_{jl}^{(r)} = \begin{cases} 2\left(A_{jj}^{(r)} A_{jl}^{(r)} - \dfrac{A_{jl}^{(r)}}{\xi_j - \xi_l}\right) & j,l=1,...,N_r \ , l \neq j \\ -\displaystyle\sum_{\substack{l=1 \\ j \neq l}}^{N_r} B_{jl}^{(r)} & for \ j=l; \ j,l=1,2,....,N_r \end{cases} \qquad (19)$$

In the similar way, the weighting coefficients can be obtained for the z-direction.

Using the 2D-GDQ method for the spatial derivatives, the discretized form of the equations of motion at each domain grid point can be obtained as shown in Appendix A. Similarly, the boundary conditions can be discretized. For this purpose, using the 2D-GDQ discretization rules for spatial derivatives, one can obtain:

For clamped edge:

$$u_{rmjk} = 0$$
$$u_{\theta mjk} = 0 \qquad (20)$$
$$u_{zmjk} = 0$$

For free edge at $r=r_i$:

$$\left(C_{11}\right)_{jk} \sum_{l=1}^{Nr} A_{jl}^r u_{rmlk} + \left(C_{12}\right)_{jk} \left(\frac{u_{rmjk}}{r_j} + \frac{m}{r_j} u_{\theta mjk}\right) +$$

$$\left(C_{13}\right)_{jk} \sum_{p=1}^{Nz} A_{kp}^z u_{zmjp} = 0$$

$$\sum_{p=1}^{Nz} A_{kp}^z u_{rmjp} + \sum_{l=1}^{Nr} A_{jl}^r u_{zmlk} = 0 \qquad (21)$$

$$-\frac{m}{r_j} u_{rmjk} + \sum_{l=1}^{Nr} A_{jl}^r u_{\theta mlk} - \frac{u_{\theta mjk}}{r_j} = 0$$

For simply support edge at $r=r_i$:

$$u_{\theta mjk} = 0$$
$$u_{zmjk} = 0$$

$$\frac{\left(C_{12}\right)_{jk}}{r_j} u_{rmjk} + \frac{m\left(C_{12}\right)_{jk}}{r_j} u_{\theta mjk} +$$

$$\left(C_{11}\right)_{jk} \sum_{l=1}^{Nr} A_{jl}^r u_{rmlk} + \left(C_{13}\right)_{jk} \sum_{p=1}^{Nz} A_{kp}^z u_{zmjp} = 0 \qquad (22)$$

For z=0, h:

$$\frac{\left(C_{23}\right)_{jk}}{r_j} u_{rmjk} + \frac{m\left(C_{23}\right)_{jk}}{r_j} u_{\theta mjk} +$$

$$\left(C_{13}\right)_{jk} \sum_{l=1}^{Nr} A_{jl}^r u_{rmlk} + \left(C_{33}\right)_{jk} \sum_{p=1}^{Nz} A_{kp}^z u_{zmjp} = 0$$

$$\sum_{p=1}^{Nz} A_{kp}^z u_{rmjp} + \sum_{l=1}^{Nr} A_{jl}^r u_{zmlk} = 0 \qquad (23)$$

$$\sum_{p=1}^{Nz} A_{kp}^z u_{\theta mjp} - \frac{m}{r_j} u_{zmjk} = 0$$

where $A_{jl}^r, A_{kp}^z, B_{jl}^r$ and B_{kp}^z are the first and second-order DQ weighting coefficients in the *r* and *z* directions, respectively. The expressions of the A_{jl}^r, A_{kp}^z, B_{jl}^r and B_{kp}^z formula are available in the literature [32, 34].

In order to carry out the eigenvalue analysis, the domain and boundary degrees of freedom are separated and described in vector forms. They are denoted by {d} and {b}, respectively. Based on these definitions, the discretized form of the motion equations and the related boundary conditions take the following forms:

Equations of motion (Appendix A):

$$[[K_{db}] \quad [K_{dd}]]\begin{Bmatrix} \{b\} \\ \{d\} \end{Bmatrix} - \omega^2 [M]\{d\} = \{0\} \qquad (24)$$

Boundary conditions (Eqs. (20)-(23)):
$$[K_{bd}]\{d\} + [K_{bb}]\{b\} = \{0\} \qquad (25)$$

Eliminating the boundary degrees of freedom in Eq. (24), using Eq. (25), this equation turns into:

$$([K] - \omega^2 [M])\{d\} = \{0\} \qquad (26)$$

where $[K] = [K_{dd}] - [K_{db}][K_{bb}]^{-1}[K_{bd}]$. The above eigenvalue system of equations can be solved to find the natural frequencies and mode shapes of the annular plates.

3. Numerical Results and Discussion

4.1 Verification of results

Free vibration analysis of Two-Dimensional Functionally Graded annular plates (2D-FG annular plate) is performed via general Differential Quadrature Method (GDQ). The equations of motion are obtained based on the 3D elasticity theory.

For this purpose, a 2D-FG annular plate with arbitrary dimension must be considered. All values including dimensions of the plate as well as frequency parameters are presented as non-dimensional form for ease of use. In order to ensure the accuracy of the results, comparisons have been performed by the literature.

Verification of the results is performed in two stages. Firstly, a homogenous and isotropic annular plate with clamped-clamped boundary condition is considered and then a free-clamped FG annular plate with conventional material distribution (Eq. (27)) is investigated.

In Tables 2 and 3, the presented results are compared with the similar ones in the literature, namely the homogenous isotropic annular plate and one-dimensional FG annular plate ($\Omega = \omega R_o \sqrt{\rho/G_m}$).

The results obtained by analysis of the 2D-GDQ for both cases are shown in Tables 2 and 3. A faster rate of convergence for the proposed 2D-GDQ procedure is obvious in comparison with Chebyshev–Ritz method ([22, 35]). Hence, a good agreement is

achieved within the results. For this verification, the number of grids in radial and thickness directions for the 2D-GDQ is assumed $N_r = N_z = 15$. The constituents of the FG annular plate in the second case are distributed according to Eq. 32 as follows:

$$E(z) = (E_m - E_c)(z/h + 0.5)^P + E_c$$
$$\rho(z) = (\rho_m - \rho_c)(z/h + 0.5)^P + \rho_c$$
$$E_m = 70Gpa, \ E_c = 380Gpa$$
$$\rho_c = \rho_m = 3800kg/m^3 \quad , v = 0.3$$

(27)

4.2 Parameter studies

In this section the effects of different parameters such as BCs as well as power exponent coefficients are studied on the natural frequency parameters. There are several efforts in which the mechanical dynamic response of FGMs has been studied, but in the case of vibration analysis of the 2D-FG plate using the 2D-GDQ method, a lack of knowledge is perceived.

Table 2. The first eight non-dimensional frequencies for the isotropic annular plates with the clamped-clamped condition
($R_o/R_i = 2.5, h/R_o = 0.5$)

m	method	Ω_1	Ω_2	Ω_3	Ω_4	Ω_5	Ω_6	Ω_7	Ω_8
0	present	4.6582	8.9505	11.3915	14.3382	17.2782	19.2184	19.4718	21.8688
	Ref. [22]	4.661	8.952	11.40	14.34	17.29	19.22	19.48	21.87
	Ref. [35]	4.660	8.950	11.40	14.34	17.28	19.22	19.48	21.87
1	present	4.7482	8.5359	9.1248	11.2232	12.7365	14.4148	16.7438	17.6333
	Ref. [22]	4.752	8.536	9.127	11.23	12.74	14.42	16.75	17.64
	Ref. [35]	4.750	8.536	9.126	11.23	12.74	14.42	16.75	17.64
2	Present	5.0865	9.0963	9.7069	11.1450	13.6461	14.6436	16.5603	18.1813
	Ref. [22]	5.089	9.097	9.709	11.15	13.65	14.65	16.56	18.18
	Ref. [35]	5.088	9.096	9.708	11.15	13.65	14.65	16.56	18.18
3	Present	5.7206	9.7439	10.5762	11.4287	14.7313	15.0190	16.5436	18.7558
	Ref. [22]	5.723	9.745	10.58	11.43	14.73	15.02	16.55	18.76
	Ref. [35]	5.722	9.744	10.58	11.43	14.73	15.02	16.55	18.76

Table 3. The first eight non-dimensional frequencies for the FGM annular plates having the free-clamped condition
($R_o/R_i = 2.5, h/R_o = 0.5$)

P	m	method	Ω_1	Ω_2	Ω_3	Ω_4	Ω_5	Ω_6	Ω_7	Ω_8
1	0	present	3.6499	8.6838	10.6489	15.0467	16.7138	17.7982	18.0660	21.0876
		Ref. [22]	3.652	8.684	10.650	15.045	16.711	17.795	18.063	21.087
	1	present	4.4508	7.2983	9.2262	10.6320	13.6344	14.1947	15.2558	16.6110
		Ref. [22]	4.453	7.298	9.226	10.632	13.633	14.193	15.255	16.608
	2	present	6.2567	7.7562	10.5431	11.5508	14.5422	15.7763	16.1538	17.0964
		Ref. [22]	6.259	7.756	10.543	11.550	14.542	15.775	16.152	17.094
	3	present	8.4036	8.9101	12.3127	13.2659	15.3383	16.6047	17.5216	18.2774
		Ref. [22]	8.406	8.910	12.313	13.265	15.338	16.602	17.519	18.275
5	0	present	4.4804	11.2575	12.5651	19.5573	21.0189	23.0737	23.5991	28.3433
		Ref. [22]	4.482	11.254	12.565	19.548	21.007	23.058	23.589	28.359
	1	present	5.4668	9.1670	11.7041	12.9115	17.2524	18.8533	19.6915	20.9746
		Ref. [22]	5.468	9.165	11.701	12.910	17.244	18.843	19.684	20.960
	2	present	7.6872	9.8504	12.9084	14.7923	18.6025	20.0166	21.4650	21.7318
		Ref. [22]	7.689	9.848	12.904	14.788	18.596	20.006	21.456	21.715
	3	present	10.3284	11.4778	14.9668	17.4532	19.5565	21.5712	22.8608	23.2461
		Ref. [22]	10.329	11.475	14.962	17.447	19.550	21.558	22.851	23.231

Table 4. The convergence study of the first three non-dimensional frequencies for the FGM annular plates having the free-clamped condition
($R_O / R_i = 2.5, h / R_O = 0.5, m = 1, P = 1$)

		Ω_1	Ω_2	Ω_3
The number of Chebyshev polynomial terms as shown in Ref. [22]	$I*J=8*4$	4.474	7.317	9.278
	$I*J=20*12$	4.453	7.298	9.227
	$I*J=30*15$	4.453	7.298	9.226
The number of nodes in GDQ method	$Nr*Nz=7*7$	4.446	7.300	9.226
	$Nr*Nz=9*9$	4.449	7.298	9.225
	$Nr*Nz=11*11$	4.450	7.298	9.226
	$Nr*Nz=13*13$	4.450	7.298	9.226

Two studies dealing with the free vibration analysis of homogenous and FG isotropic annular plates are presented in previous section in order to validate the results. Hence, we are satisfied with the results which are presented in previous section. Two functions of constituent distribution namely exponential and power law introduced and presented in previous section, reveal the functionality of material distribution with respect to the radial and thickness directions.

It is assumed that the plate stands in ambiance temperature with different mechanical boundary conditions are introduced in section 2. The significant difference within the numerical results is revealed in the rate of convergence. The generalized differential quadrature method due to the few number of grids, for convergence and also the accurate solutions in comparison with other numerical methods is more popular.

Fig. 5 shows the rate of convergence for the first natural frequency of the annular plate obtained in terms of different values of N_r when N_z has specified constant values.
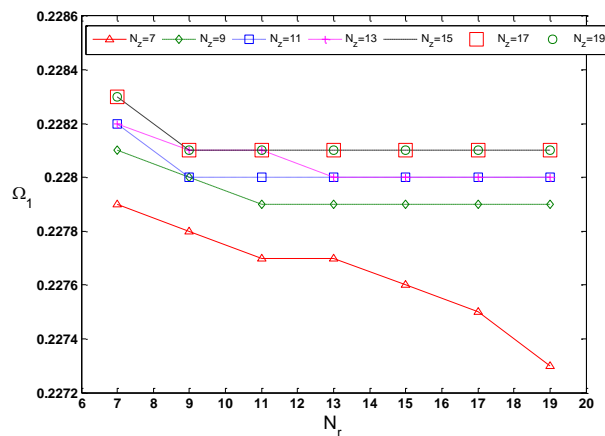
Figure 5. The effect of the GDQ grids on the rate of convergence for the first natural frequency, h=0.2, $\lambda_1 = \lambda_2 = 1$, r_i/r_o=0.2

According to the figure, reasonable converged results and accurate natural frequency are obtained in at least 15 nodes along the thickness and 9 nodes along the radius directions and that would be acceptable in differential quadrature method. Moreover, Table 4 compares accuracy and convergence rate of the presented method and a popular numerical method for frequency analysis of the FGM annular plates. In this table, 30*15 number of Chebyshev polynomial terms in Chebyshev-Ritz is tantamount to 11*11 nodes in the GDQ method for analysis of the first three natural frequencies in the FGM annular plates which means the GDQ method solves fewer equations and consequently it leads to accurate answers faster than the other method.

Meshing the plate in two directions and using the 2D-GDQ procedure lead to obtain more accurate result with a fast rate of convergence. Also, the 3D graphs are employed in order to investigate the rate of convergence for this algorithm. The number of points required for convergence in radius and thickness directions is studied and the rate of convergence for the first three non-dimensional natural frequencies in terms of different numbers of nodes in radial (N_r) and thickness (N_z) directions is shown in Fig. 6. The flat part of each figure in Fig. 6 (a-c) shows the first three frequencies achieve convergence for a certain number of nodes along the r and z directions.

In other words, significant changes in response to increasing the number of nodes in the two-dimensional grid have not been observed. For example, in Fig. 6 (a) per nine nodes in the r direction and 15 nodes along the z direction the first frequency converges, or in the case of Fig. 6 (c) per 9 nodes along the r direction and 11 nodes along the z direction the third frequency converges. As it is observed, the convergence is fast and a few numbers of grid points along the radial and thickness directions are required ($N_r = 9$, $N_z = 15$). Variations of the first non-dimensional natural frequencies versus the material graded index (or power coefficients) in case of conventional FG annular plate along the thickness or radial and the 2D-FG annular plate in both directions, for different boundary conditions are demonstrated in Figs. (7-9) (r_i=0.2, r_o=1, h=0.2) . Figs. 7-8 depict the first non-dimensional natural frequency variations of conventional FG annular plate versus the variation of the power coefficients along the thickness and radial directions, in terms of different boundary conditions, respectively.

Fig. 7 shows variation of the frequency versus the power coefficient for conventional FG annular plate, in which the materials are graded throughout the thickness direction. It is observed that the frequency tends to decrease when the power coefficient increases. Also, for a plate with fully clamped edges, the highest natural frequency is obtained. Additionally, the slop of frequency graph decreases for a plate with fewer constraints i.e. here the F-C plate is less than other types of boundary conditions.

In Fig. 9, it is assumed $\lambda_1 + \lambda_2 = 8$. It is observed that the boundary conditions have significant effects on natural frequency parameter of the FG annular plate. For the case of functionally graded plate along the radial direction, the frequency variation is quiet different. As it is observed, the first non-dimensional natural frequency of the annular plate under all boundary conditions except (S-S) increases with an increase in the functionally graded index in radial direction, but under (S-S) condition, it reduces.

(a)

(b)

(c)
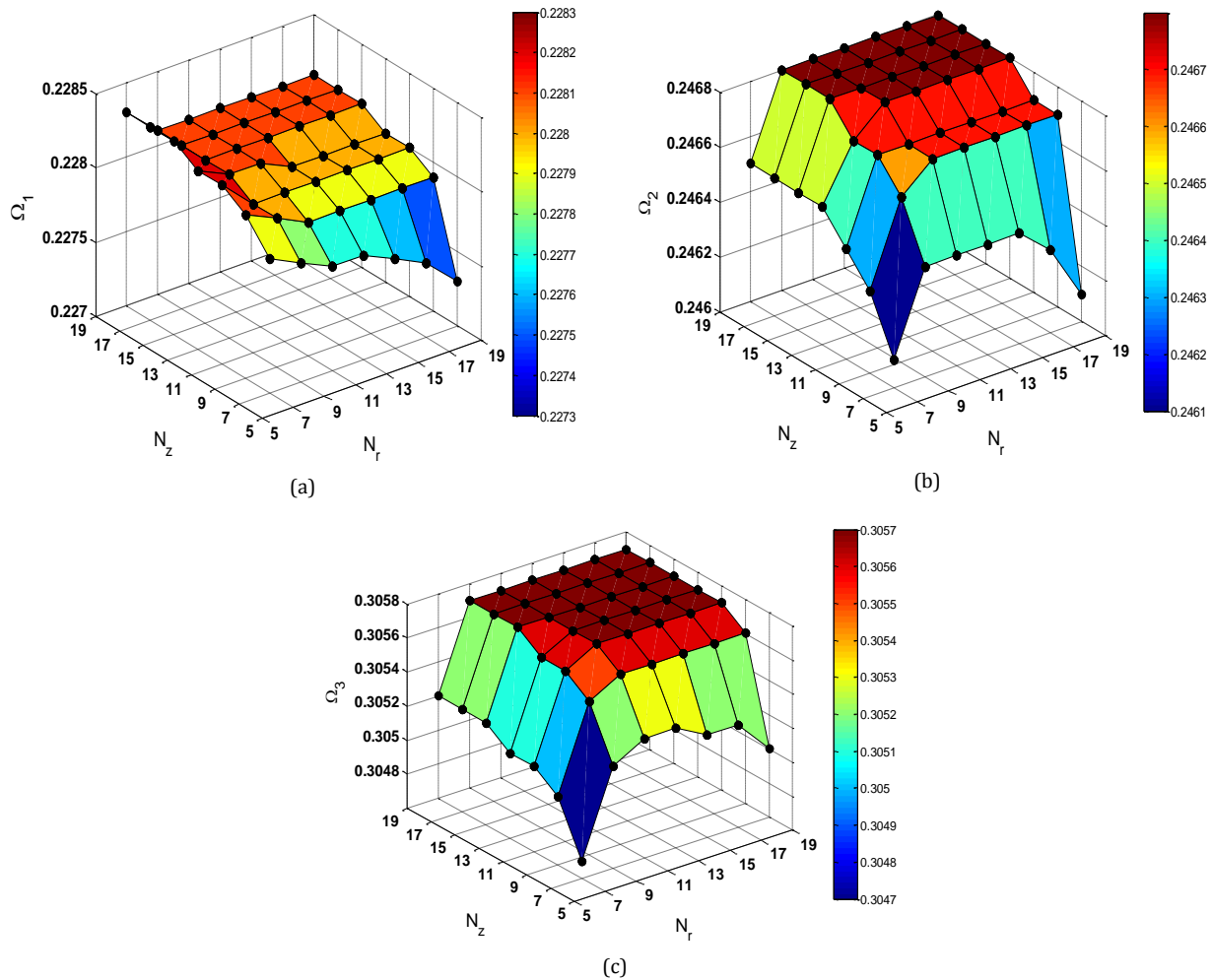
Figure 6. The rate of convergence for the first three natural frequencies in case of simply supported–clamped condition, *h*=0.2, $\lambda_1 = \lambda_2 = 1$, r_i/r_o=0.2

Fig. 9 for the 2D-FGM shows a same behavior for all boundary conditions, the first non- dimensional natural frequency gradually increases with an increase in the ratio of the radial to thickness graded indices. It should be noticed, for an annular plate with a material property graded index in radial direction lower than 2 (Fig. 8), and for a 2D-FGM with a material graded index ratio almost less than 0.5 (Fig. 9), the first non-dimensional natural frequency under (S-S) boundary condition is higher than the natural frequency under (F-C) condition. For the 2D-FGM in case of (S-S) condition, the first non-dimensional natural frequency is almost constant for a material graded index ratio greater than 1. The effects of plate thickness on the first non-dimensional natural frequency for conventional FG annular plate graded along thickness, or radial direction and 2D-FG annular plate under different boundary conditions including (C-C),(F-C),(S-C) and (S-S) are shown in Figs. 10-12, respectively (r_i =0.2, r_o=1).

Figs. 10 and 11 show the non-dimensional natural frequency variations of uni-directional FGM in thickness or radial directions, respectively, versus the material property graded index under different boundary conditions. The aforementioned graded index in the thickness and radial directions has an insignificant effect on the first non-dimensional natural frequency of thin plates (h/R_o=0.05). In case of the thin 2D-functionally graded annular plate in Fig. 12, the first non-dimensional natural frequency gradually increases and then remains almost constant for the ratio of the radial to thickness graded indices around 1, it remains almost constant.

Fig. 13 (a-e) shows the first non-dimensional natural frequency variations versus n_r and n_z parameters for 5 considered models illustrated in Fig. 3. It should be noted, the dynamic behavior of two models (1) and (3) are similar and the first natural frequency increases with the increase in n_r and n_z parameters. It could be as a result of the increase in the plate stiffness. In model (5), a similar behavior is shown. However, more variation of the first natural frequency is observed with the increase in n_z at constant n_r. The dynamic behavior of model (2) with respect to n_r and n_z parameters variation is similar with model (4) with respect to n_z and n_r, respectively. According to Fig. 13 (a-e), one can obtain an appropriate design for the 2D-FGM arrangement among different possible cases for a variety range of applications. The behaviors of the first and third kinds of these arrangements are similar, but the other kinds present different characteristics which can be used for different goals.
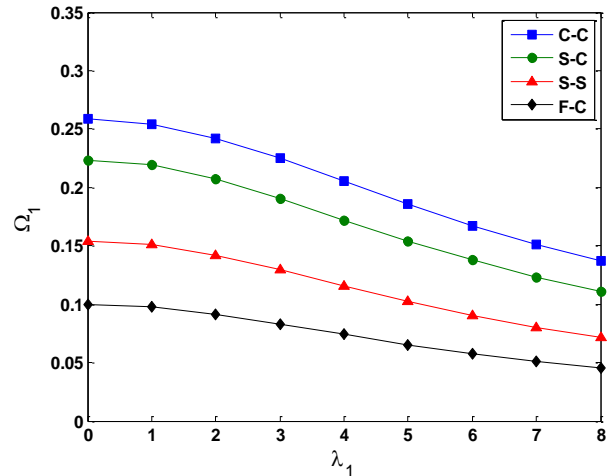
Figure 7. The variations of the first non-dimensional natural frequency parameter for the 1D-FGM versus the graded index in the thickness direction ($\lambda_2 = 0$)
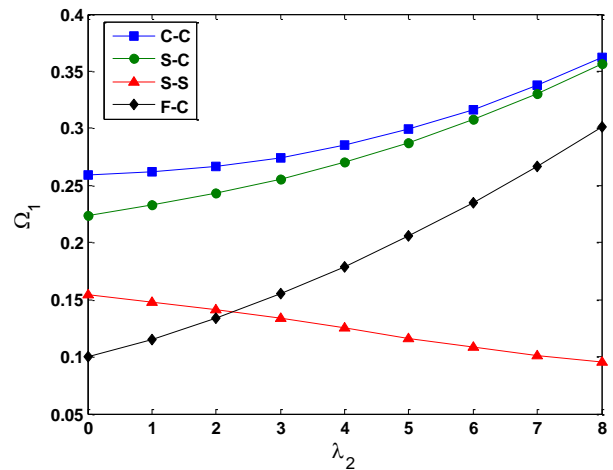
Figure 8. The variations of the first non-dimensional natural frequency parameter for the 1D-FGM versus the graded index in the radial direction ($\lambda_1 = 0$)
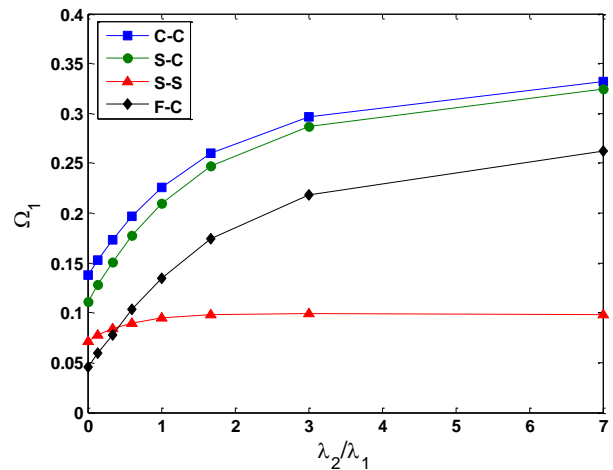
Figure 9. The variations of the first non-dimensional natural frequency parameter versus the ratio of the radial graded index to the thickness graded index for the 2D-FGM
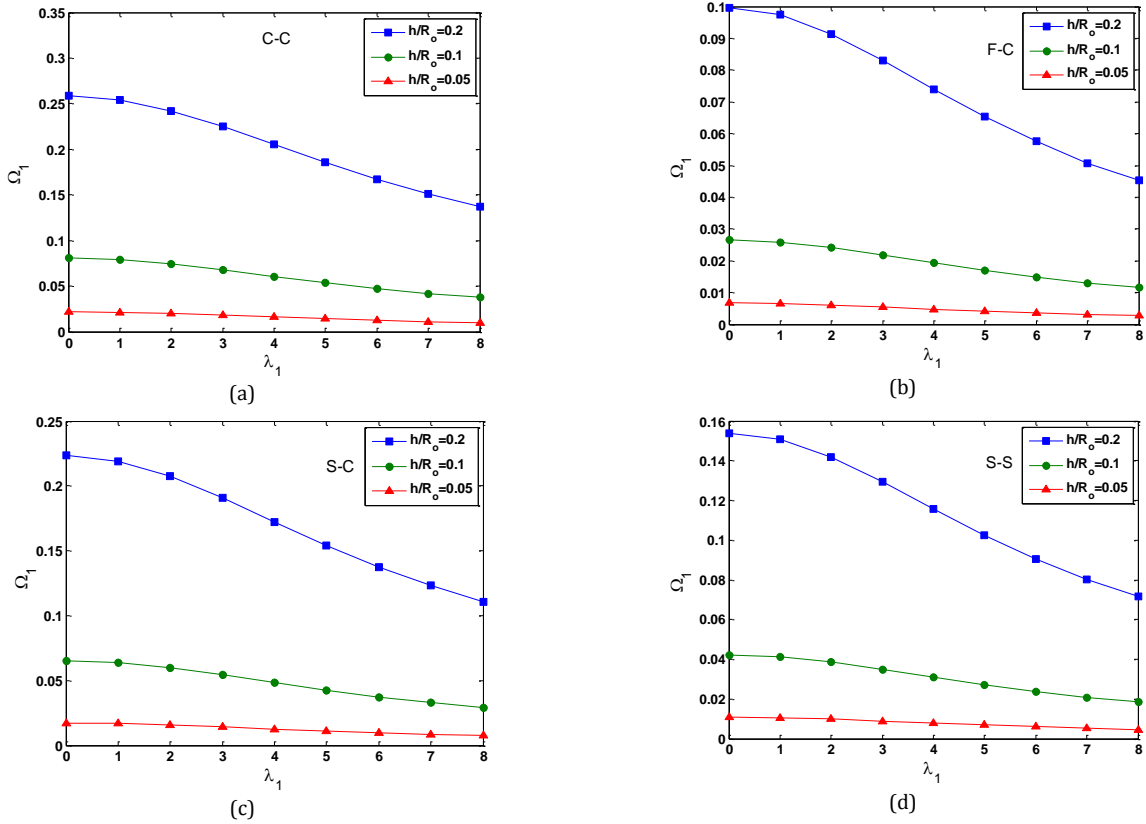
Figure 10. The variations of the first non-dimensional natural frequency parameter versus the graded index in the thickness direction ($\lambda_2 = 0$) under a-(C-C), b-(F-C), c-(S-C), d-(S-S) boundary conditions
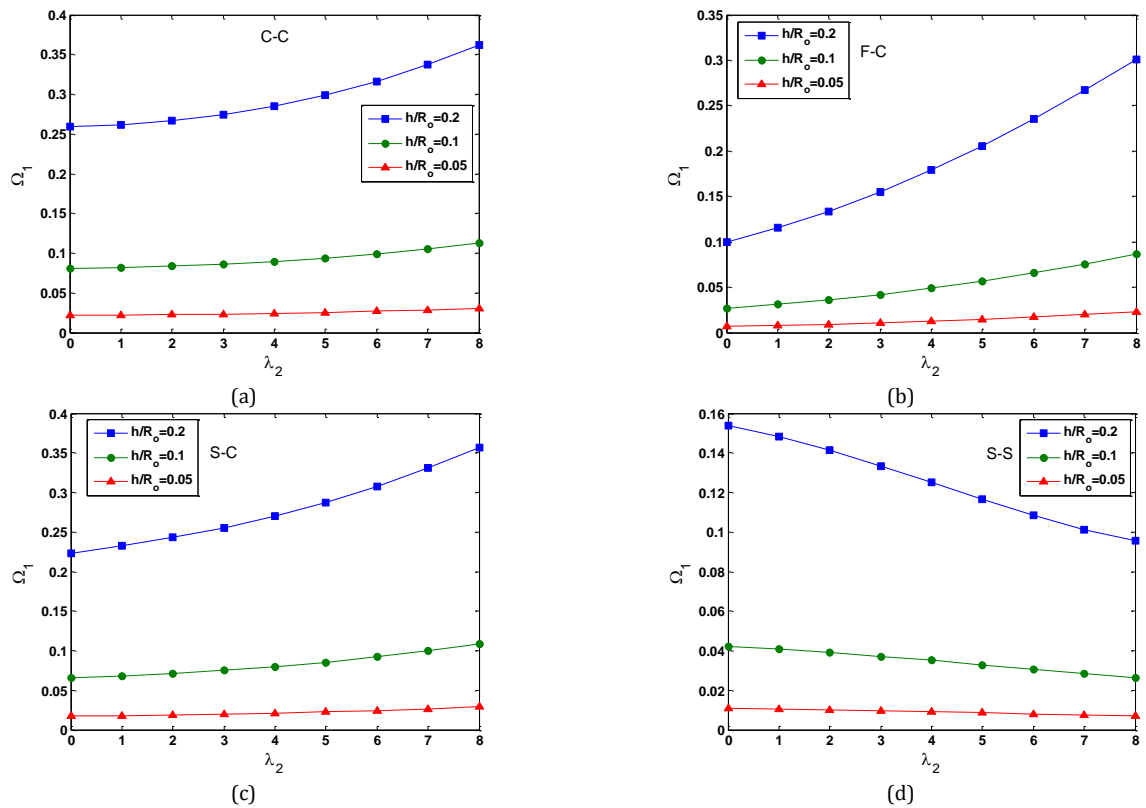
Figure 11. The variations of the first non-dimensional natural frequency parameter versus the graded index in the radial direction ($\lambda_1 = 0$) under a-(C-C), b-(F-C), c-(S-C), d-(S-S) boundary conditions
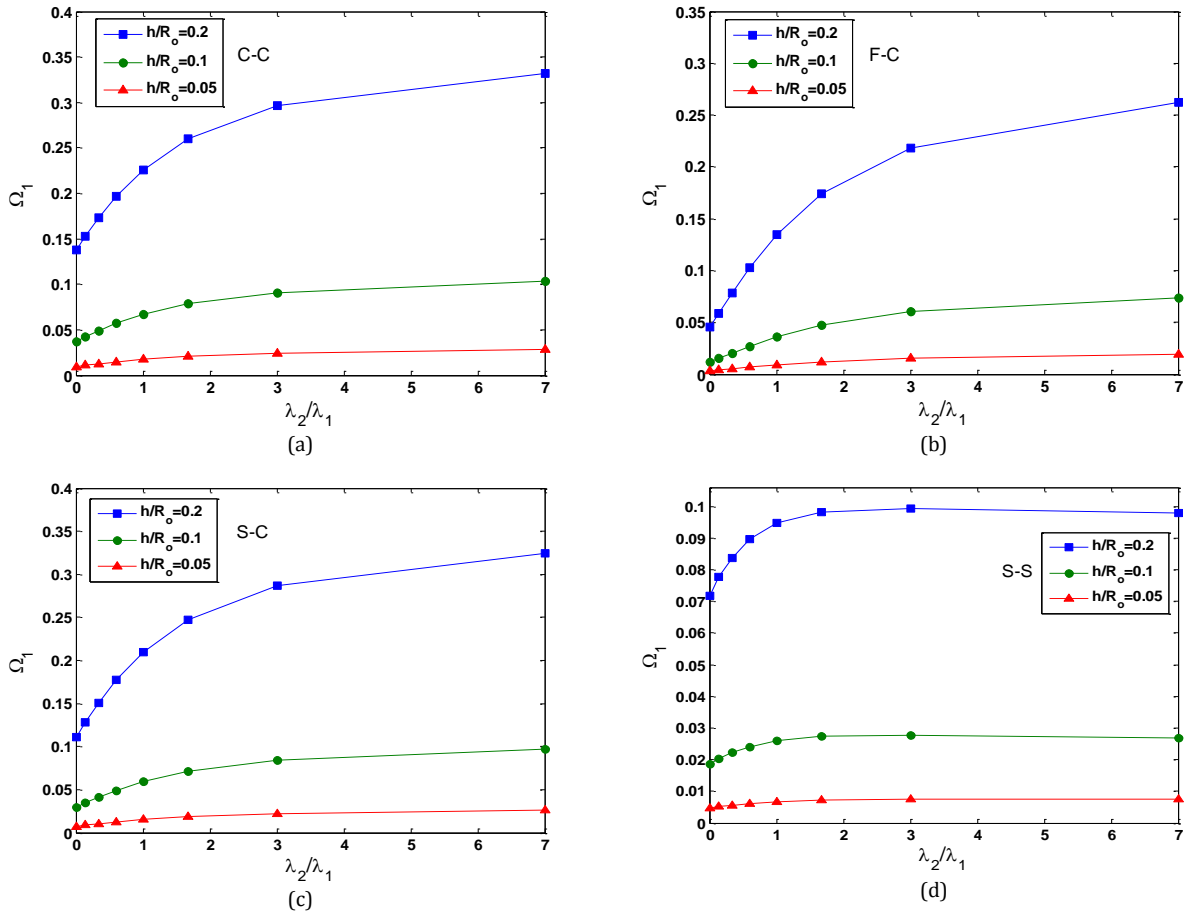
Figure 12. The variations of the first non-dimensional natural frequency parameter versus the ratio of the radial graded index to the thickness graded index for the 2D- FGM under a-(C-C), b-(F-C), c-(S-C), and d-(S-S) boundary conditions
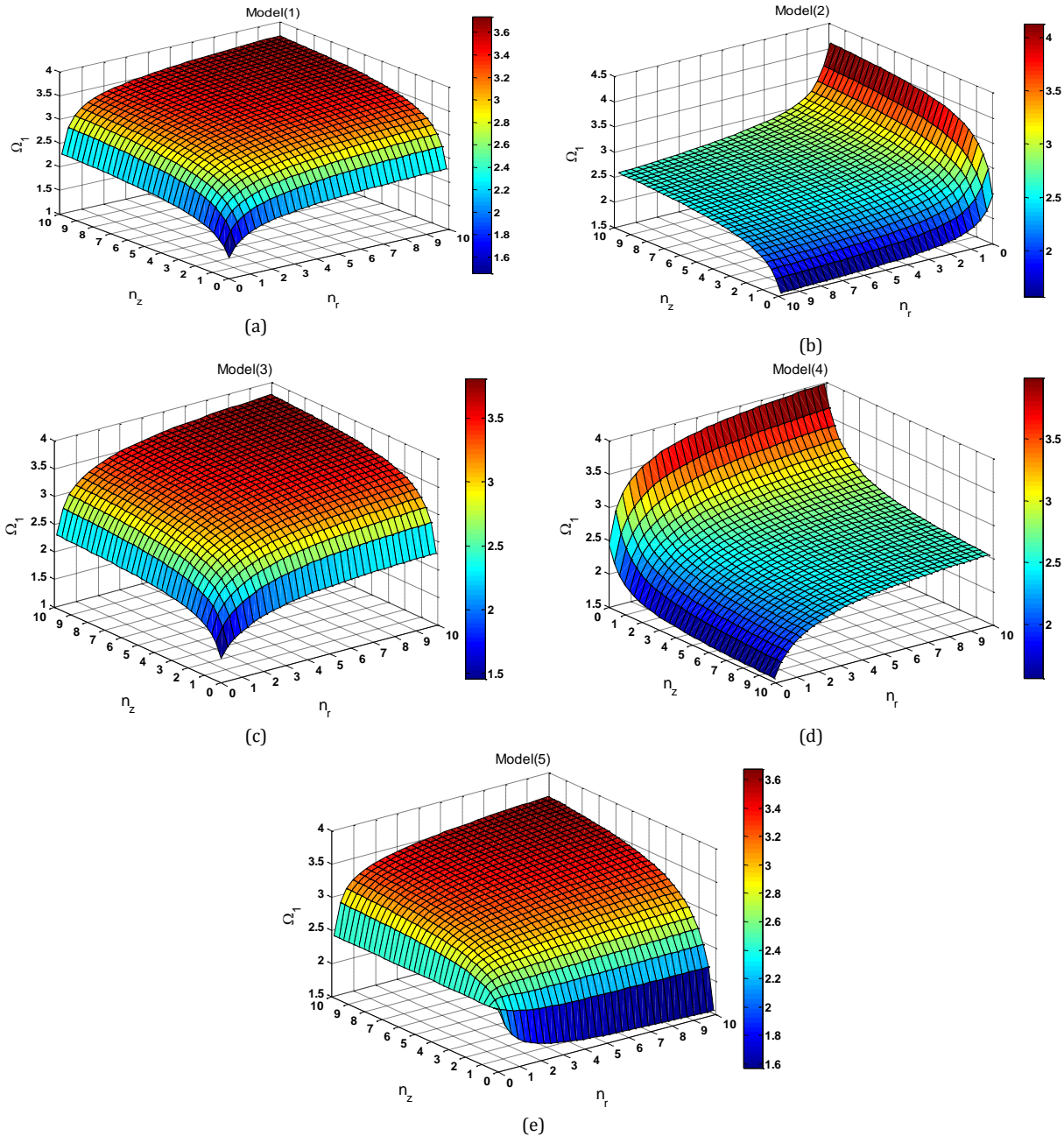
Figure 13. The behavior of the first non-dimensional natural frequency versus the material property graded indexes for different models, a-model (1), b-model (2), c-model (3), d-model (4), and e-model (5)

5. Conclusions

The mechanical free vibration of the 2D-FG annular plates was investigated using the Generalized Differential Quadrature method (GDQ) based on the two-dimensional meshing. The three-dimensional elasticity theory was employed in order to derive equations of motion for the 2D-FG annular plates. The mechanical properties of the 2D-FG annular plate were assumed to be temperature independent since only the mechanical vibration analysis was performed. The material constituents were distributed as the function of *r* and *z* coordinates simultaneously by the power law and exponential formulation.

A semi-analytical approach composed of two-dimensional generalized differential quadrature methods (2D-GDQ) and series solution were adopted to solve the equations of the motion. The effect of the functionality of the material properties on the position, boundary conditions including simply supported-clamped, clamped-clamped, free-clamped and simply supported-simply supported in inner and outer radii, respectively as well as the aspect ratio were taken into account, too.

The results for the natural frequency parameter of the 2D-FG annular plate with different parameters have illustrated the fast convergence and high accuracy of the proposed approach in terms of using 2D grids. From this study, the following conclusion can be remarked:

- The convergence of the 2D-GDQ method is fast and the results have a good agreement with the previous investigations.
- The different distributions of four kinds of materials, according to the rule of mixture to form an annular plate with variable properties in two directions are employed. The results show different or same dynamic behaviors in terms of different arrangement of materials and it could be seen.

For the exponential distribution, it is concluded that:

- In terms of the functionally graded indexes in thickness or radial directions increase, the first non-dimensional natural frequencies increase for all kinds of boundary conditions, but (s-s) boundary condition for the uni-directional FGM annular plate in radial direction, shows subtractive trend.
- Increasing the geometrical thickness parameter leads to an increase in the first dimensionless frequency for all kinds of boundary conditions.
- The non-dimensional natural frequencies of thin uni-directional functionally graded along the radial or thickness directions as well as the thin 2D-FGM annular plate according to Figs.(10-12) depend on the functionally graded indices in thickness and radial directions, however, their variation against these parameters is small.
- For the 2D-FGM under (S-S) condition, the first non-dimensional natural frequency is almost constant for the material graded index ratio which is greater than 1.

References

[1] Brush DO, Almorth BO. **Buckling of bars, plates and shells**, McGraw-Hill, 1975.

[2] Finot M, Suresh S. Small and large deformation of thick and thin-film multilayers: effect of layer geometry, plasticity and compositional gradients, *J Mech Phys Solids* 1996; 44(5): 683–721.

[3] Pan E, Han F. Exact solution for functionally graded and layered magnetoelectro- elastic plates, *Int J Eng Sci* 2005; 43(3-4): 321–339.

[4] Cheng ZQ, Batra RC. Deflection relationships between the homogeneous Kirchhoff plate theory and different functionally graded plate theories, *Arch Mech* 2000; 52(1): 143–158.

[5] Bhangale RK, Ganesan N. Static analysis of simply supported functionally graded and layered magneto-electro-elastic plates, *Int J Solid Struct* 2006; 43(10): 3230–3253.

[6] Ramirez F, Heyliger PR, Pan E. Discrete layer solution to free vibrations of functionally graded magneto-electro-elastic plates, *Mech Adv Mater Struct* 2006; 13(3): 249–266.

[7] Abrate S. Free vibration, buckling, and static deflections of functionally graded plates, *Compos Sci Technol* 2006; 66(14): 2383–2394.

[8] Hosseini-Hashemi S, Rokni Damavandi Taher H, Akhavan H, Omidi M. Free vibration of functionally graded rectangular plates using first-order shear deformation plate theory, *Appl Math Modell* 2010; 34(5): 1276–1291.

[9] Kim YW. Temperature dependent vibration analysis of functionally graded rectangular plates, *J Sound Vib* 2005; 284(3-5): 531–549.

[10] Malekzadeh P. Three-dimensional free vibration analysis of thick functionally graded plates on elastic foundations, *Compos Struct* 2009; 89(3): 367–373.

[11] Yas MH, Sobhani Aragh B. Free vibration analysis of continuous grading fiber reinforced plates on elastic foundation, *Int J Eng Sci* 2010; 48(12): 1881–1895.

[12] Chiroiu V, Munteanu L. On the free vibrations of a piezoceramic hollow sphere, *Mech Res Commun* 2007; 34(2): 123–129.

[13] Chen WQ. Vibration theory of non-homogeneous, spherically isotropic piezoelastic bodies, *J Sound Vib* 2000; 236(5): 833–860.

[14] Haddadpour H, Mahmoudkhani S, Navazi HM. Free vibration analysis of functionally graded cylindrical shells including thermal effects, *Thin-Walled Struct* 2007; 45(6): 591–599.

[15] Sobhani Aragh B, Yas MH. Three-dimensional free vibration of functionally graded fiber orientation and volume fraction cylindrical panels, *Mater Des* 2010; 31(9): 4543–4552.

[16] Yas MH, SobhaniAragh B. Three-dimensional analysis for thermoelastic response of functionally graded fiber reinforced cylindrical panel, *Compos Struct* 2010; 92(10): 2391–2399.

[17] Bahtui A, Eslami MR. Coupled thermoelasticity of functionally graded cylindrical shells, *Mech Res Commun* 2007; 34(1): 1–18.

[18] Prakash T, Ganapathi M. Asymmetric flexural vibration and thermoelastic stability of FGM circular plates using finite element method, *Compos Part B* 2006; 37(7-8): 642–649.

[19] Eraslan AN, Akis T. On the plane strain and plane stress solutions of functionally graded rotating solid shaft and solid disk problems, *Acta Mech* 2006; 181(1-2): 43–63.

[20] Efraim E, Eisenberger M. Exact vibration analysis of variable thickness thick annular isotropic and FGM plates, *J Sound Vib* 2007; 299(4-5):720–738.

[21] Nie GJ, Zhong Z. Semi analytical solution for three-dimensional vibration of functionally graded circular plates, Comput. *Methods Appl Mech Eng* 2007; 196(49-52): 4901–4910.

[22] Dong CY. Three-dimensional free vibration analysis of functionally graded annular plates using the Chebyshev–Ritz method, *Mater Des* 2008; 29(8): 1518–1525.

[23] Tahouneh V, Yas MH. 3-D Free vibration analysis of thick functionally graded annular plates on Pasternak elastic foundation via differential quadrature method (DQM), *Acta Mech* 2012; 223(9): 1879-1897.

[24] Hosseini-Hashemi S, Fadaee M, Atashipour SR. A new exact analytical approach for free vibration of Reissner-Mindlin functionally graded rectangular plates, *Int J Mech Sci* 2011; 53(1): 11–22.

[25] Jodaei A, Jalal M, Yas MH. Free vibration analysis of functionally graded annular plates by state-space based differential quadrature method and comparative modeling by ANN, *Compos Part B* 2012; 43(2): 340–353.

[26] Malekzadeh P, Shahpari SA, Ziaee HR. Three-dimensional free vibration of thick functionally graded annular plates in thermal environment. *J Sound Vib* 2010; 329(4): 425–42.

[27] Rad AB, Shariyat M. A three-dimensional elasticity solution for two-directional FGM annular plates with non-uniform elastic foundations subjected to normal and shear tractions, *Acta Mech Solida Sinica* 2013; 26(6): 671–90.

[28] Malekzadeh P, Safaeian Hamzehkolaei N. A 3D discrete layer-differential quadrature free vibration of multi-layered FG annular plates in thermal environment, *Mech Adv Mater Struct* 2013; 20(4):316-30.

[29] Liang X, Kou H, Wang L, Palmer AC, Wang Z, Liu G. Three-dimensional transient analysis of functionally graded material annular sector plate under various boundary conditions. *Compos Struct* 2015; 132(15): 584–596.

[30] Nie G, Zhong Z. Dynamic analysis of multi-directional functionally graded annular plates, *Appl Math Modell* 2010; 34(3): 608–616.

[31] Asgari M, Akhlaghi M. Natural frequency analysis of 2D-FGM thick hollow cylinder based on three-dimensional elasticity equations, *Eur J Mech A/Solids* 2011; 30(2):72–81.

[32] Bert CW, Malik M. Differential quadrature method in computational mechanics: A review, *Appl Mech* 1996; 49(1): 1–28.

[33] Bellman RF, Kashef BG, Casti J. Differential quadrature: A technique for the rapid solution of nonlinear partial differential equations, *Comput Phys* 1972; 10(1): 40–52.

[34] Shu C. **Differential Quadrature and Its Application in Engineering**, Springer Publication, 2000.

[35] Zhou D, Au FTK, Cheung YK, Lo SH. Three-dimensional vibration analysis of circular and annular plates via the Chebyshev-Ritz method, *Int J Solid Struct* 2003; 40(12): 3089–3105.

Appendix A

$$\left(\frac{\partial C_{11}}{\partial r}\right)_{jk}\sum_{l=1}^{Nr} A_{jl}^r u_{rmlk} + (C_{11})_{jk}\sum_{l=1}^{Nr} B_{jl}^r u_{rmlk} + \left(\frac{\partial C_{12}}{\partial r}\right)_{jk}\left(\frac{u_{rmjk}}{r_j}\right) + \left(\frac{\partial C_{13}}{\partial r}\right)_{jk}\sum_{p=1}^{Nz} A_{kp}^z u_{zmjp} + (C_{13})_{jk}\sum_{l=1}^{Nr}\sum_{p=1}^{Nz} A_{kp}^z A_{jl}^r u_{zmlp} +$$

$$\frac{(C_{12})_{jk}}{r_j}\left(m\sum_{l=1}^{Nr} A_{jl}^r u_{\theta mlk}\right) - \frac{(C_{12})_{jk}}{r_j^2}\left(mu_{\theta mjk}\right) + \left(\frac{\partial C_{12}}{\partial r}\right)_{jk}\frac{m}{r_j}u_{\theta mjk} + \frac{(C_{66})_{jk}}{r_j}\left(m\sum_{l=1}^{Nr} A_{jl}^r u_{\theta mlk}\right) + \frac{(C_{12})_{jk}}{r_j}\sum_{l=1}^{Nr} A_{jl}^r u_{rmlk}$$

$$+\left(\frac{\partial C_{55}}{\partial z}\right)_{jk}\left(\sum_{p=1}^{Nz} A_{kp}^z u_{rmjp}\right) - \frac{(C_{66})_{jk}}{r_j}\frac{m}{r_j}u_{\theta mjk} - \frac{(C_{12})_{jk}}{r_j^2}u_{rmjk} - \frac{(C_{23})_{jk}}{r_j}\sum_{p=1}^{Nz} A_{kp}^z u_{zmjp} - \frac{(C_{12})_{jk}}{r_j}\sum_{l=1}^{Nr} A_{jl}^r u_{rmlk} -$$

$$\frac{(C_{22})_{jk}}{r_j}\left(\frac{m}{r_j}u_{\theta mjk}\right) + (C_{55})_{jk}\left(\sum_{l=1}^{Nr}\sum_{p=1}^{Nz} A_{kp}^z A_{jl}^r u_{zmlp}\right) + \frac{(C_{11})_{jk}}{r_j}\sum_{l=1}^{Nr} A_{jl}^r u_{rmlk} + \frac{(C_{12})_{jk}}{r_j}\left(\frac{U_{rmjk}}{r_j} + \frac{m}{r_j}u_{\theta mjk}\right) +$$

$$\frac{(C_{13})_{jk}}{r_j}\sum_{P=1}^{Nz} A_{kp}^z u_{zmjp} + (C_{55})_{jk}\sum_{p=1}^{Nz} B_{kp}^z u_{rmjp} - \frac{(C_{22})_{jk}}{r_j}\frac{u_{rmjk}}{r_j} + \left(\frac{\partial C_{55}}{\partial z}\right)_{jk}\sum_{l=1}^{Nr} A_{jl}^r u_{zmlk} - \frac{(C_{66})_{jk}}{r_j}\frac{m^2}{r_j}u_{rmjk} = -\rho_{jk}\omega_m^2 u_{rmjk}$$

(A1)

$$\left(\frac{\partial C_{66}}{\partial r}\right)_{jk}\left(-\frac{m}{r_j}u_{rmjk}\right) - (C_{66})_{jk}\frac{1}{r_j}\sum_{l=1}^{Nr} A_{jl}^r u_{\theta mlk} + (C_{66})_{jk}\frac{m}{r_j^2}u_{rmjk} - \frac{m(C_{12})_{jk}}{r_j}\sum_{l=1}^{Nr} A_{jl}^r u_{rmlk} - \frac{m(C_{23})_{jk}}{r_j}\sum_{P=1}^{Nz} A_{kp}^z u_{zmjp}$$

$$+\left(\frac{\partial C_{66}}{\partial r}\right)_{jk}\sum_{l=1}^{Nr} A_{jl}^r u_{\theta mlk} + \left(\frac{\partial C_{44}}{\partial z}\right)_{jk}\sum_{P=1}^{Nz} A_{kp}^z u_{\theta mjp} - \frac{m^2(C_{22})_{jk}}{r_j^2}u_{\theta mjk} + (C_{66})_{jk}\left(-\frac{m}{r_j}\sum_{l=1}^{Nr} A_{jl}^r u_{rmlk}\right) + \left(\frac{\partial C_{44}}{\partial z}\right)_{jk}\left(-\frac{m}{r_j}u_{zmjk}\right)$$

$$+(C_{44})_{jk}\left(-\frac{m}{r_j}\sum_{P=1}^{Nz} A_{kp}^z u_{zmjp}\right) + (C_{66})_{jk}\sum_{l=1}^{Nr} B_{jl}^r u_{\theta mlk} - \frac{2m(C_{66})_{jk}}{r_j^2}u_{rmjk} + \frac{2(C_{66})_{jk}}{r_j}\sum_{l=1}^{Nr} A_{jl}^r u_{\theta mlk} - \frac{2(C_{66})_{jk}}{r_j^2}u_{\theta mjk} - \frac{m(C_{22})_{jk}}{r_j^2}u_{rmjk}$$

$$-\left(\frac{\partial C_{66}}{\partial r}\right)_{jk}\frac{u_{\theta mjk}}{r_j} + (C_{66})_{jk}\frac{1}{r_j^2}u_{\theta mjk} + (C_{44})_{jk}\sum_{p=1}^{Nz} B_{kp}^z u_{\theta mjp} = -\rho_{jk}\omega_m^2 u_{\theta mjk}$$

(A2)

$$\left(\frac{\partial C_{55}}{\partial r}\right)_{jk}\left(\sum_{p=1}^{Nz} A_{kp}^z u_{rmjp}\right) + (C_{55})_{jk}\left(\sum_{l=1}^{Nr}\sum_{p=1}^{Nz} A_{kp}^z A_{jl}^r u_{rmlp}\right) + \frac{m(C_{44})_{jk}}{r_j}\sum_{p=1}^{Nz} A_{kp}^z u_{\theta mjp} - \frac{m^2(C_{44})_{jk}}{r_j^2}u_{zmjk} + \left(\frac{\partial C_{13}}{\partial z}\right)_{jk}\sum_{l=1}^{Nr} A_{jl}^r u_{rmlk}$$

$$+(C_{13})_{jk}\sum_{l=1}^{Nr}\sum_{p=1}^{Nz} A_{kp}^z A_{jl}^r u_{rmlp} + \frac{1}{r_j}\left(\frac{\partial C_{23}}{\partial z}\right)_{jk}\left(u_{rmjk}\right) + (C_{55})_{jk}\sum_{l=1}^{Nr} B_{jl}^r u_{zmlk} + \left(\frac{\partial C_{55}}{\partial r}\right)_{jk}\sum_{l=1}^{Nr} A_{jl}^r u_{zmlk} + \frac{(C_{23})_{jk}}{r_j}\left(\sum_{p=1}^{Nz} A_{kp}^z u_{rmjp}\right)$$

$$+\left(\frac{\partial C_{33}}{\partial z}\right)_{jk}\sum_{p=1}^{Nz} A_{kp}^z u_{zmjp} + \frac{1}{r_j}\left(\frac{\partial C_{23}}{\partial z}\right)_{jk} mu_{\theta mjk} + (C_{33})_{jk}\sum_{p=1}^{Nz} B_{kp}^z u_{zmjp} + \frac{(C_{55})_{jk}}{r_j}\sum_{p=1}^{Nz} A_{kp}^z u_{rmjp} + \frac{(C_{55})_{jk}}{r_j}\sum_{l=1}^{Nr} A_{jl}^r u_{zmlk} +$$

$$\frac{(C_{23})_{jk}}{r_j} m\sum_{p=1}^{Nz} A_{kp}^z u_{\theta mjp} = -\rho_{jk}\omega_m^2 u_{zmjk}$$

(A3)